

Joint Analysis of the Wind and Wave-Field Variability in the Indian Ocean Area For 1998–2009¹

F. Pogarskii^a, V. Polnikov^a, and S. A. Sannasiraj^b

^a *Obukhov Institute of Atmospheric Physics, Russian Academy of Sciences, Moscow, Russia*

^b *Indian Institute of Technology of Madras, Chennai, India*

e-mail: polnikov@mail.ru

Received April 28, 2011; in final form, December 29, 2011

Abstract—In this paper, a detailed statistical analysis of the wind and wave fields in the Indian Ocean (IO) for the period of 1998–2009 was performed based on using the wind fields taken from the site of the National Centers for Environmental Prediction and the National Oceanic and Atmospheric Administration (NCEP/NOAA) [1] and on the numerical wind-wave model WAM [2] modified with the source function proposed in [3]. The primary analysis of the fields includes mapping the wind and wave fields, as well as their energy fields, calculated with different scales of space-time averaging; the subsequent zoning of the IO area; and assessing the seasonal interannual variability of all the fields and their 12-years trends. Further analysis is carried out taking into account the zoning. This analysis includes a construction of the time series obtained with different scales of space-time averaging for all the fields, a spectral analysis of these series, finding and analyzing the spatial and temporal distribution of extrema of the wind and wave fields (accounting for the their sharing in the zones), and making histograms of the wind and wave fields and calculating their first four statistical moments (in the zones and in the ocean as a whole). The results allow us to evaluate a large set of statistical characteristics of the wind and wave fields in the IO area, scales of their variability, their long-term trends, and the features of distribution for these statistical characteristics in the ocean area as well.

Keywords: Indian Ocean, wind and wave fields, density of flux for a kinetic energy of wind, wave-energy density, spectra of time series, spatial and temporal variability, histograms, statistical moments.

DOI: 10.1134/S0001433812060114

1. INTRODUCTION

This paper represents a stage of implementation of the international Russian–Indian (Russian Federation of Basic Research project no. 10-05-92662-IND_a) study devoted to wind and wind-wave fields and their energy store, as well as the processes of their interaction, and the long-term variability of these fields using the example of the Indian Ocean (IO). Because the wind field is the primary source of all processes mentioned above, a study of its variability and statistical characteristics is primary and obligatory. After that, the WAM wind-wave model [2] modified with the new source function [3] was used to calculate the wind-wave fields. To solve the problems of the project, in this paper we proposed a certain methodical approach for processing geophysical fields which will be used later as the reference approach for processing fields of other variables planned in the further implementation of this project.

The wind field $\mathbf{W}(x, y, t)$ used in this study is defined as a three-dimensional array for two compo-

nents of the wind vector. It was obtained from the site of the National Centers for Environmental Prediction and the National Oceanic and Atmospheric Administration (NCEP/NOAA) [1]. The field represents a reanalysis prepared with the following sizes of the space-time grid: 1° in latitude, 1.25° in longitude, and 3 h in time. The accuracy of the field components is on the order of 1.5–2 m/s (estimations found in paper [4] and archive [5]). At the time the work was conducted, the available period of reanalysis was 12 years: 1998–2009.

Such a detailed and long-term wind field, to our knowledge, has not been used for a detailed study of its statistics in the IO yet, despite the fact that such works have a long history and have been successfully carried out in many research centers around the world for different areas of the World Ocean (references see in [6–10]). The objectives of our work do not include any detailed analysis of the previous results, because our project focuses mainly on a study of features for a space-time structure of the wind- and wave-field energy, as well as their long-term trends, and the variability of intensity for their mechanical interaction on long-term scales. Such an approach to a study of the

¹ The article was translated by the authors.

air–sea interaction is unique and has no analogues. Therefore, for our purposes, the abovementioned works are used as certain reference points only, permitting us to control the quality of our results that overlap with those mentioned above.

In addition, it is essential to note that another distinctive feature of our study is a detailed account of the spatial inhomogeneity of the wind field in the IO. The accounting this circumstance is achieved by zoning the entire ocean area into a number of zones that differ in wind-field dynamics. As the basis of zoning, we use the stable distributions of local extrema for the averaged wind field (see below). Introducing zoning allows us to detect the characteristics of the wind-field variability in the area studied with a greater certainty and in more detail than the results found in earlier studies [6–10].

Sections 2–6 are devoted to analyzing the wind field in the IO, while sections 7–10 are devoted to a wave-field analysis.

2. THE TASKS SET FORTH

Using the example of the wind field, the general formulation of the main sets of tasks is stated as follows.

(1) To build and analyze four types of charts for the mean wind field, $\langle W(i, j, T) \rangle$, given by the formula

$$\langle W(i, j, T) \rangle = \left(\sum_{t_n \in T} \Delta t_n W(i, j, t_n) \right) / \sum_{t_n \in T} \Delta t_n, \quad (2.1)$$

where $\Delta t_n = \Delta t = 10800$ s is the time step, T is the period of averaging, and $W(i, j, t_n)$ is the wind module at the spatial node (i, j) at the time moment t_n . The following constructions are made: (a) charts for a certain winter (January) and summer (July) month averaged over all years and a chart of the seasonal variability, (b) one-year-averaged charts and the charts of the interannual variability, (c) a chart of the wind field averaged for the entire period, and (d) a chart of the mean wind-field trend for the entire period.

The purpose is to define the seasonal and interannual variability of the mean wind values, the 12-year trend of the wind field, and the spatial distribution of the latter. Based on an analysis of the spatial distribution of the wind, the justification of IO zoning is to be executed.

(2) To build and analyze charts of the mean densities of the horizontal flux for a kinetic energy of wind (hereinafter, FKEW), $\langle E_A(i, j, T) \rangle$, given by the formula

$$\langle E_A(i, j, T) \rangle = \left(\sum_{t_n \in T} \Delta t_n \rho_a W^3(i, j, t_n) / 2 \right) / \sum_{t_n \in T} \Delta t_n, \quad (2.2)$$

where $\rho_a = (353/T_K)$ kg/m³ is the air density taken with account for its dependence on climatic mean temperature T_K (in the Kelvin scale), varying with the latitude and seasons. Variations of the argument T in (2.2) correspond to the four types of averaging mentioned in task 1.

The goal is to estimate the FKEW quantities in the zones and in the whole IO and their variation with the seasons and years and define the 12-year trend of FKEW and its spatial distribution. The FKEW is estimated in units of the power per unit of a vertical square (Wt/m²) located perpendicular to the wind direction. The significance of the FKEW is stipulated for the fact that it is what characterizes the rate of transfer of the mechanical energy from wind to waves [11].

(3) To construct graphs of a time history for the mean wind speed $W(R, T)$ and mean FKEW $E_A(R, T)$ averaged over space and time and defined by the relations

$$W(R, T, t) = \left(\sum_{t_n \in T} \Delta t_n \sum_{i, j \in R} W(i, j, t_n) \Delta S_{ij} \right) / \sum_{t_n \in T} \Delta t_n / \sum_{i, j \in R} \Delta S_{ij}, \quad (2.3)$$

$$E_A(R, T)$$

$$= \left(\sum_{t_n \in T} \Delta t_n \sum_{i, j \in R} \frac{\rho_a}{2} W^3(i, j, t_n) \Delta S_{ij} \right) / \sum_{t_n \in T} \Delta t_n / \sum_{i, j \in R} \Delta S_{ij},$$

where ΔS_{ij} is the grid-cell square of the IO area adjacent with the left lower corner to the i th node of latitude and to j th node of longitude. The argument R is the index of the spatial integration (i.e., the fixed point, the zone, or the whole ocean); the argument T means the period of averaging.

The following 12-year series are constructed: (a) the time history for the “instantaneous” (3-h time step) values of $W(R, T, t)$ and $E_A(R, T, t)$ at the fixed points of zones, (b) the time history of the same quantities made with the 1-day averaging (1-day time step) and with averaging over each of the zones, and (c) the time history of the same quantities with the 1-day averaging and averaging over the whole IO. All the resulting time series are subjected to spectral analysis. The goal is to determine the scales of temporal variability for the “instantaneous” magnitudes of wind and FKEW at the fixed points and the same magnitudes averaged over the zones and over IO as the whole.

(4) To construct the time-history graphs for the mean wind, $W(R, T, t)$ and mean FKEW $E_A(R, T, t)$ with the annual averaging (for each year of 1998–2009) for each zone and for the whole IO. The goal is to define the 12-year trends for the 1-year mean wind speed and FKEW averaged both over zones and the whole IO.

(5) To determine the extreme values of wind $W_{\max}(i_m, j_m, t_m)$ and their spatial and temporal location

i_m, j_m, t_m for each zone. To build a chart of the extreme values $W_{\max}(i, j)$ found for each point of the IO area studied. The goal is to provide information about the real values of the wind maxima, including their time and space locations.

(6) To construct a set of histograms for the wind speed: (a) for the entire period 1998–2009 at the individual (distinguished) points of each zone, (b) for a dedicated winter (January) and summer (July) month with accumulation for the whole period (for each zone), and (c) for all years with the space integration over each zone separately and over the whole IO.

The goal is to demonstrate evidently the spatial and temporal variability of the distribution function for the wind module and the dependence of the former on the scale of averaging.

(7) For all kinds of histograms referred to in item 6, to calculate four statistical moments (mean, standard deviation, skewness, and kurtosis) and to estimate parameters of the empirical distribution function as parameterized by the Weibull distribution.

The goal is to demonstrate the extent of correspondence of the statistical characteristics mentioned to those known from literature [8–10].

The specificity of the analysis is to study the statistics of the wind field and FKEW for three types of spatial scales: at each point of the ocean (charts), the zonal distribution of characteristics, and the integral values of characteristics. This approach is consistent with the principle of enlarging the scale of describing the geophysical field. In the following presentation of results, we will adhere to this principle. Due to the limited size of this paper, the results will be given in a visual form for the most important items of the above problems only. A lot of omitted results are available when accessing archive [5] or directly from the authors.

3. ANALYSIS OF THE CHARTS FOR WIND AND WIND ENERGY

3.1. The Mean Wind Charts

A chart of wind speed $\langle W(i, j, T) \rangle$ averaged for the entire period is shown in Fig. 1a. An analysis of all the charts of such a kind shows the following features of the mean wind fields. First, all the maps show a clear and stable distribution of wind speed in space like one shown in Fig. 1a. Taking the presence of local extrema in the wind field as a basis for zoning, the following areas could be distinguished: the Arabian Sea (Z1), the Bay of Bengal (Z2), the equatorial part of IO (Z3), the southern part of the trade wind in IO (Z4), the southern subtropical part of IO (Z5), and the southern IO (Z6). Such a distribution of extremes for the wind field indicates the stability of the spatial dynamics of atmospheric circulation over the IO as a whole. The bound-

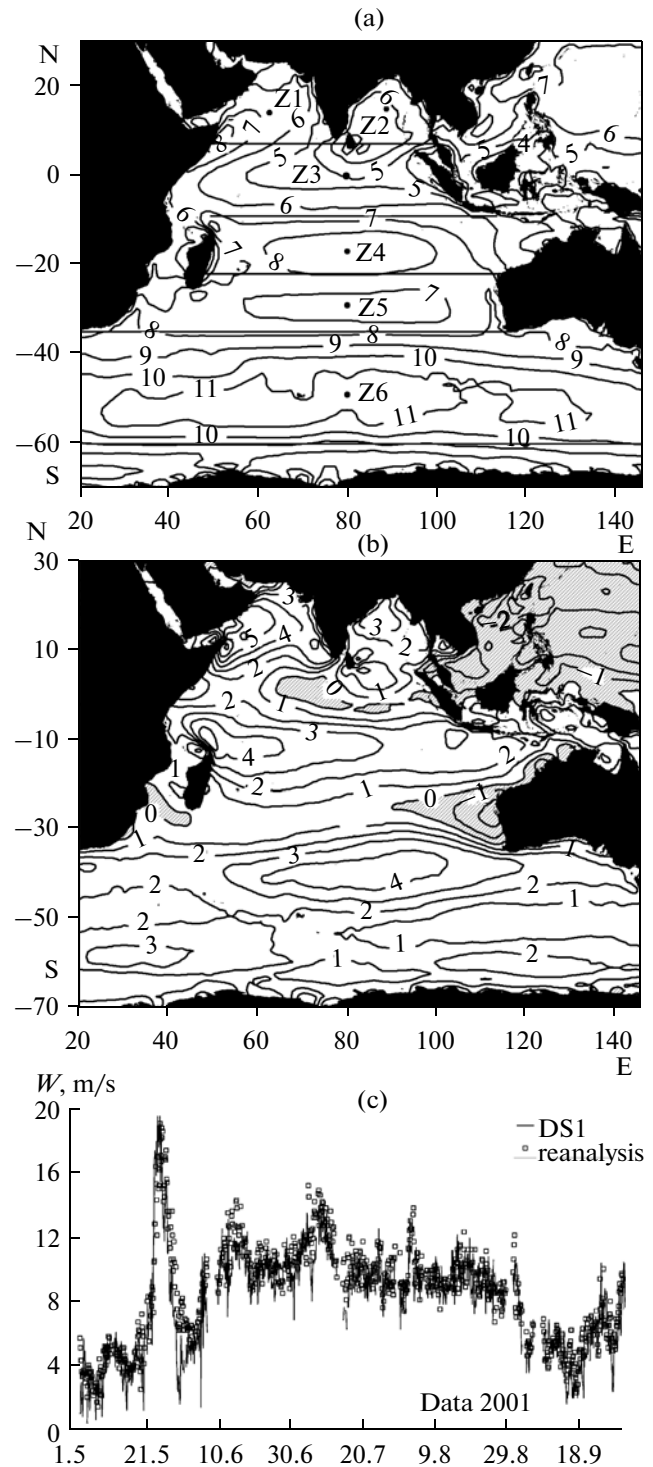


Fig. 1. (a) The field of mean wind speed for the entire period of 1998–2009 (straight lines indicate the boundaries of the selected zones Z1–Z6 of the IO zoning; the bold dots denote the “central” points of the zones), m/s; (b) The field of seasonal difference of the season-mean fields (July–January) averaged over the entire period, m/s (the areas of negative values in the seasonal differences are shaded); (c) the 3-h-value history of the wind speed at buoy DS1 and the appropriate reanalysis data at the proper grid point for the period from May to September 2001.

The coordinates of buoys and the mean-square-root errors δH_S for model calculations of wave height H_S for the two variants of the WAM model and three buoys in the IO

Buoy index [buoy coordinates]	δH_S , m	
	WAM-orig	WAM- modif
DS1 [15.5° N; 69.3° E]	0.75	0.47
DS2 [10.7° N; 72.5° E]	0.40	0.29
SW3 [15.4° N; 73.7° E]	0.45	0.28
Mean error	0.533	0.347

aries of zones and the location of their “central” points are shown in Fig. 1a by thick straight lines and dots, respectively (numerical values are given in the table of archive [5]).

For completeness, we note that the average values of wind-speed range from a minimum of 4–6 m/s in equatorial zone Z3 to a maximum of 12–14 m/s in zone Z6. Herewith, the maximum wind values are often achieved just in the summer (Fig. 1b in [5]).

The exact values of the winds averaged over all ocean zones are given in archive [5]. It is interesting to note the strong seasonal variability of the mean wind field shown using the example of “summer–winter” variability (Fig. 1b). Almost everywhere except for zones of weak winds, Z3 and Z5, the increase in average winds is remarkable in the summer time; it is especially noticeable in the western parts of zones Z1 and Z3. According to our estimates, this growth can reach 7–8 m/s, which is associated with the monsoon dynamics taking place in the northern part of the IO. The negative value of the seasonal difference taking place near the western coast of Australia (zone Z5) and reaching up to $-(3-4)$ m/s apparently has a similar nature. The temporal trend, obtained by the method of least squares for each point of the wind field, is characterized by chaotic heterogeneity (Fig. 1 in [5]), slightly resembling Fig. 1a. Its analysis is given in archive [5]. It marked an increase in the average wind speed on the order of 0.06–0.08 m/s per year, especially in the areas of high winds (zones Z1, Z4, and Z6). There are also weak negative trends (in the centers of zones Z3 and Z5, as well as in the center and to the east of zone Z6) reaching values of -0.04 m/s per year. The reliability of the established trend is small, because the latter is within confidence intervals having a value of $\Delta_w \cong 0.05$ m/s (for details, see [5]). For a more reliable determination of trends (and their explanation), a greater period of analysis is evidently required.

Note: To confirm the applicability of the wind fields for dynamics analysis and for the further analysis of wind-wave fields calculated for this wind, a compar-

ison was performed between the wind speed measured at three buoys (coordinates are given in table) and the wind values of reanalysis at the corresponding grid points. In Fig. 1c a plot of this comparison for a buoy called DS1 is shown. One can see a good coincidence of the values of wind speed (correlation coefficient $K_{\text{corr}} = 0.90$ and standard deviation $\delta W = 1.5$ m/s). Taking into account the corrections of the buoy wind speed from a height of $H = 3$ m to a height of $H = 10$ m, the values of the mean wind speed for reanalysis and the one measured at the buoy are 8.2 and 8.5 m/s, respectively. This evaluation confirms the high quality of reanalysis.

3.2. The Charts of the Flux of Kinetic Energy of Wind

The charts of FKEW $\langle E_A(i, j, T) \rangle$ in general repeat the main features of the wind field $\langle W(i, j, T) \rangle$, essentially emphasizing the zones of extreme winds. The expediency of studying the FKEW comes from the determining role of this characteristic in the process of interaction between the atmosphere and ocean [11, 12]. For this reason, as the basis of our studying the wind field, we study the time-space distribution of the flux of kinetic energy of wind and its variability. The additional specificity of the FKEW assessment $\langle E_A(i, j, T) \rangle$ is given by an account for the air density dependence on the temperature $\rho_a(T_k)$. We achieved this accounting on the basis of data received from the report of the European Centre for Medium Range Weather Forecasts [13]. The abovementioned situation demonstrates a high self-sufficiency and importance of the FKEW field analysis. To our knowledge, there are no analogues of such calculations and their analysis in the literature.

Some results of the FKEW field calculations are shown in Figs. 2a and 2b. They testify to the following.

All the features of the spatial variability of the wind field $\langle E_A(i, j, T) \rangle$ become more emphasized in the field of wind energy flux density $\langle W(i, j, T) \rangle$. Thus, the range of variation of the FKEW field $\langle E_A(i, j, T) \rangle$ averaged for the entire period reaches up to 13 times (with a maximum of about 1300 W/m² in zone Z6, Fig. 2a). The values that were found have a pioneering nature and are of considerable interest both for evaluating the mechanical energy of the wind over IO and for describing the dynamics of interaction between the atmosphere and ocean (see Section 8).

The quantitative estimates of seasonal, interannual, and long-term variability of the FKEW fields $\langle E_A(i, j, T) \rangle$ are equally interesting (see details in [5]). Thus, the range of seasonal variation reaches values of about 100 W/m² in the minimum of FKEW and 1000 W/m² in the maximum (Fig. 2b). However, the trend of the average field $\langle E_A(i, j, T) \rangle$ has a range of $[-10, +50]$ W/m² per year; i.e., it has an order of 1%

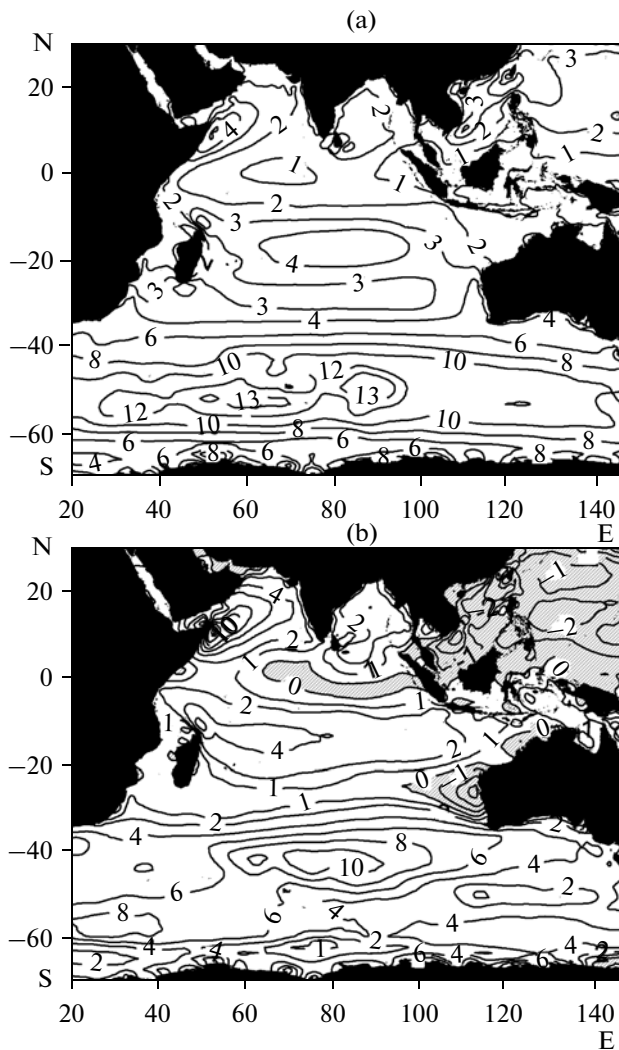


Fig. 2. (a, b) The same as in Figs. 1a and 1b, but for the average wind energy, in units of 10^2 W/m^2 .

per year (Fig. 2c [5]). That is beyond the confidence interval for these series (the statistical trend-coefficient has a value $R^2 = 0.65$, which corresponds to the criterion of its validity). Herewith, the main increase in the FKEW takes place in the central and Middle Eastern parts of zone Z6, while a weak negative trend is typical for the equatorial zone Z3 and the Far Eastern part of zone Z6. The causes of the negative trend are to be found later in the general dynamics of the spatial variability of atmospheric circulation.

4. ANALYSIS OF TEMPORAL VARIATIONS OF WIND AND ITS POWER: THE SCALES OF THEIR VARIABILITY

4.1. Time History of Wind Speed at Fixed Points of Zones

The typical time history of the “instantaneous” wind speed $W(Z_I, t)$ (time step is 3 h) (in our case, it is

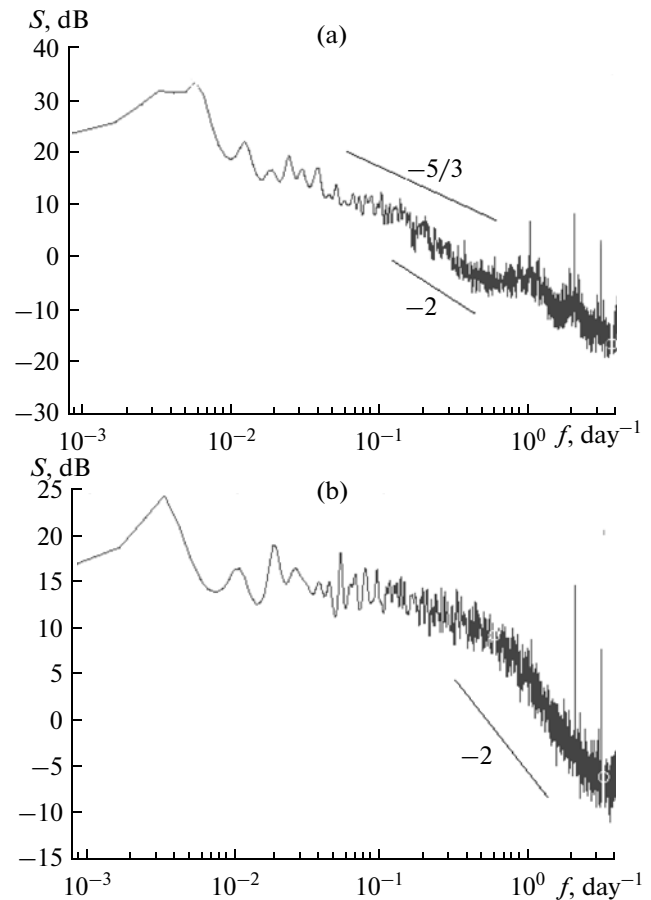


Fig. 3. The spectra of the 3-h series of wind speed at the central points (Table 1 of the archive [5]) of IO zones: (a) zones Z1 and (b) Z6.

related to the “central” points of IO’s Z_I zones, the coordinates of which are given in Table 1 of the archive [5]) shows its variation while moving to the south (see Fig. 3 in the appendix of [5]). If the northern zones are characterized by a marked irregularity of the chronogram (i.e., the presence of several visually distinguishable scales of considerable variability: weeks, season, half a year, year), only 1-year variability is noticeable in the southern IO. These visual conclusions are fully supported by the results of a spectral analysis of the series $W(Z_I, t)$ (Fig. 3).

A spectral analysis of the time series was performed using the method of autoregressive Yule–Walker analysis described in detail in [14]. According to [14], the confidence intervals Δ_S in the logarithmic coordinates scale are on the order of $\pm 10\text{--}20\%$, depending on the length of the series. Visually, this corresponds to the thickness of the smearing of the spectral line at high frequencies (with periods of 1 day or less). From an analysis of a complete set of graphs for the frequency spectra $S(\omega)$ (see [5]), we can draw the following conclusions.

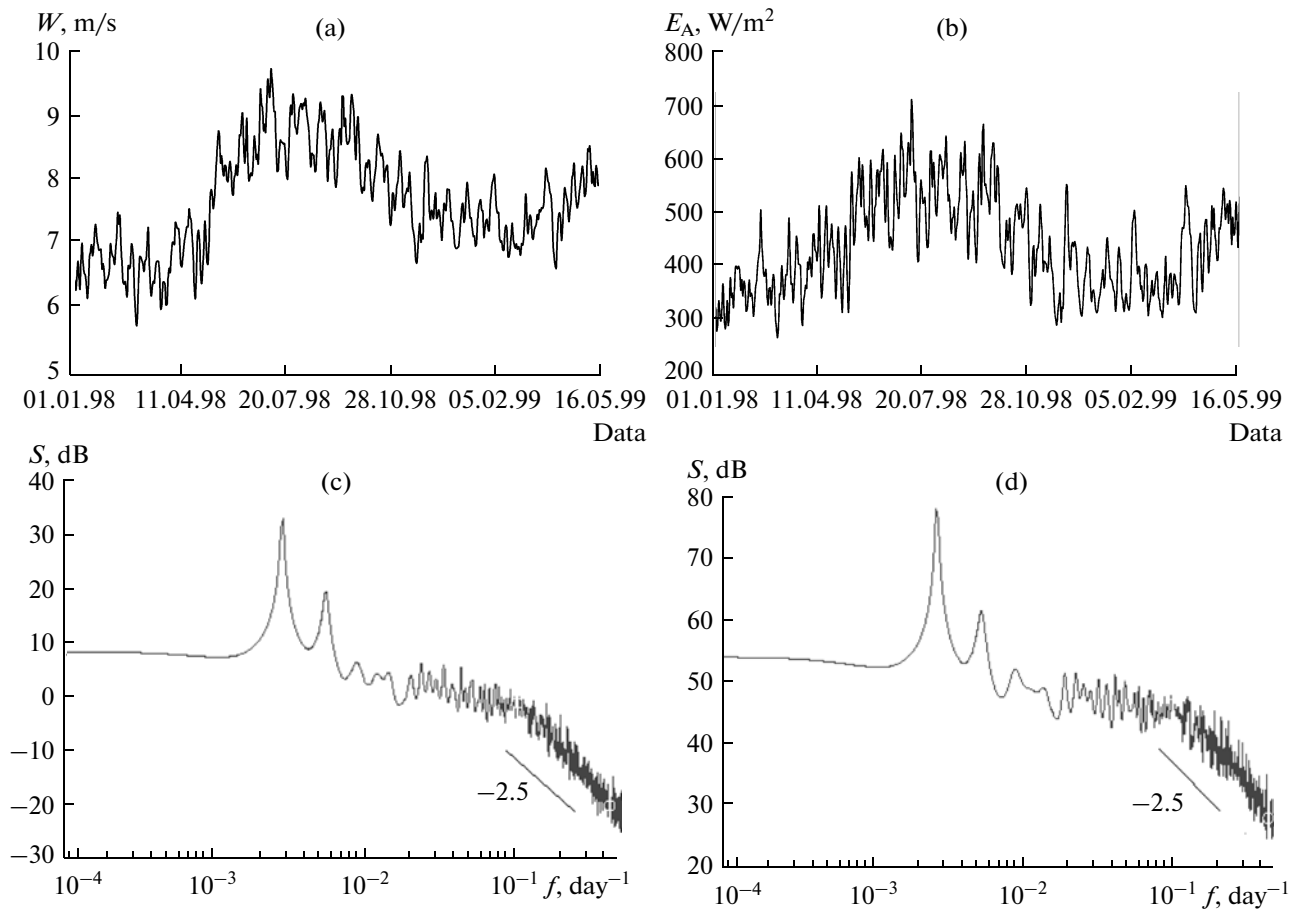


Fig. 4. The series of (a) speed and (b) energy of the wind averaged for one day and over whole IO and their spectra: (c) and (d), respectively.

For zone Z1 (Fig. 3a) and for the similar zone Z2, the greatest wind variation occurs at the period of 0.5 year. From this scale there is an almost uniformly dropping-down spectrum up to a 1 day scale, having a number of weak (but significant) peaks at periods of 100 (seasons), 30, and 15 days (mesoscales). On average, from scales of 100 days up to 1 day, the decay law of the spectrum has a form $S(\omega) \propto \omega^{-1.6 \pm 0.2}$, similar to the law of the decay for isotropic turbulence spectra, “ $-5/3$ ”, or to the spectra of Lagrangian turbulence, “ -2 ” [15]. On smaller scales there are sharp (and reliable) peaks at periods of 1, 0.5, and 0.3 days. For zone Z3, this general shape of the spectrum $S(\omega)$ is retained, but a significant peak at a period of 40 days is seen and fluctuations on scales of 1, 0.5, and 0.3 days significantly stand out.

For southern zones Z4–Z6 (Fig. 3b) there is a well-distinguished annual maximum, beyond which, at scales from 100 to 10 days there is the white noise spectrum (“shelf”), followed at high frequencies by the power-law spectrum of the form $S(\omega) \propto \omega^{-2 \pm 0.2}$, which has a decay rate slightly greater than “ $-5/3$.”

On the tail of the spectrum, there are very sharp peaks at scales of 1, 0.5, and 0.3 days.

4.2. Time History and Spectra of the FKEW at Fixed Points of Zones

It is interesting to compare the above results with those for the flux of wind energy $E_A(Z_I, t)$. The corresponding results are shown in Fig. 4 of archive [5].

According to these results, the intensity of the annual harmonic becomes dominant even for the northern zones Z1–Z3. Starting from the period of 100 days, the spectrum gradually decreases with the same “classical” law $S(\omega) \propto \omega^{-1.5 \pm 0.2}$, revealing well-marked maxima on scales of 1, 0.5, and 0.3 days.

For the southern zones Z4–Z6, all spectra have main maximum on the scale of a year, followed by a “shelf” (i.e., the spectrum of white noise) on scales from 100 to 10 days (in zone Z4) or less (up to 3 days in zone Z6). On smaller scales, this shelf is transformed into the turbulence spectrum with a slope on the order of “ -2 ” (in the spectra of all the zones). As

before, sharp peaks stood out at the scales of 1, 0.5, and 0.3 days (especially strong in zone Z4).

4.3. Time History of FKEW Averaged for a Day and over the Zones

An analysis of data of this kind shows that, when moving to the south, the semiannual variability, which is remarkable in areas of Z1–Z3, becomes weaker. But at the same time, the annual variability of wind power is well-expressed in all zones (figures of the series are given in the appendix to archive [5]). This visual analysis is confirmed by a spectral analysis (see Figs. 5 in [5]). In zones Z1–Z3, the spectra of the time-series for FKEW contain sharp peaks at periods of 1 and 0.5 year, which are replaced by a smooth decline of intensity in the range of scales from 60 days to 10 days, where the slope of the spectrum is of the form $S(\omega) \propto \omega^{-1.6 \pm 0.3}$. On scales of 10 days or less, the slope of the spectrum becomes steeper: $S(\omega) \propto \omega^{-2.5 \pm 0.5}$. In addition, in the spectra for zones Z2, Z3, there is a remarkable local maximum at the period of 40 days, which is gradually shifted to the period of 60 days as it moves to the south (to zones Z4–Z6). On the smaller scales, the white noise spectrum is achieved, located between this moving local maximum and periods of 10 days. For shorter periods, it is replaced by a falling spectrum of the kind $S(\omega) \propto \omega^{-2.5 \pm 0.5}$.

4.4. Time History of Wind and FKEW Averaged Over the Whole Ocean

In conclusion, it is interesting to point out peculiarities in the time history and spectra of the daily mean values $W(R, T, t)$ and $E_A(R, T, t)$ averaged across the whole IO (Fig. 4).

First, despite the large scale of spatial averaging, the time history of the average values $W(R, T, t)$ and $E_A(R, T, t)$ shows a very strong variability. Namely, on the synoptic scale (5–10 days), the wind averaged over the ocean can vary up to 1.3–1.4 times, whilst the average FKEW varies even up to 1.5 times (Figs. 4a, 4b). Such a strong variability of the FKEW for the whole ocean is seen as a new and quite unexpected result. Apparently, this is associated with the passage of great cyclones in the southern part of the IO.

Second, the spectra of these series (Figs. 4c, 4d) have sharply marked periods of 1 and 0.5 year. Then, the long “shelf” of the intensity of the spectrum takes place from the period of 100 to 10 days, which is followed by a rather abrupt power-law decay of the kind $S(\omega) \propto \omega^{-2.5 \pm 0.3}$. It should be noted that spectra of this kind are obtained for the first time.

Third, on the tails of the spectra, there are remarkable peaks corresponding to the scales of 8–7 days and 5–3 days. Despite the fact that these peaks are “drowning” in the statistical noise of the spectral esti-

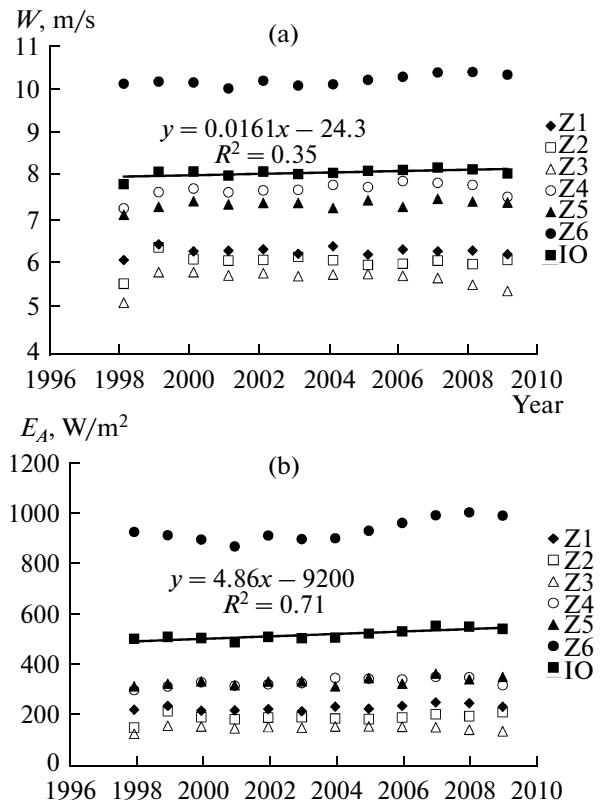


Fig. 5. The time history of (a) velocity and (b) energy of the wind averaged for 1 year and over the zones (including the mean over entire area of the IO as the average for all zones). The m.s.r. trend-lines for the entire IO and their formulas are shown.

mate, it appears that these features of the spectrum correspond to the above-noted sharp synoptic variability in the time-history series for the FKEW of the whole ocean. The general analysis and conclusions of this subsection are given in Section 6 and, in more detail, in [5].

5. ANALYSIS OF INTEGRAL AND POINT FEATURES

5.1. The Time History of the Annual Values

The two panels of Fig. 5 show the time history of the wind speed (5a) and FKEW (5b) averaged over all zones and the IO. The expected distribution of mean values among the zones is seen. Note that the estimates of annual values of FKEW averaged over the zones correspond to dependence of $E_A(R, T, t) \cong (0.8 - 0.9)W^3(R, T, t)$ 10% with an error. This empirical fact can be used for quick “expert” estimates of the mean values of FKEW without involving cumbersome calculations using formula (2.4). Restricting our analysis by the integral values for the whole IO only, we should note the presence of a barely discernible trend for the averaged wind speed: growth on the order of

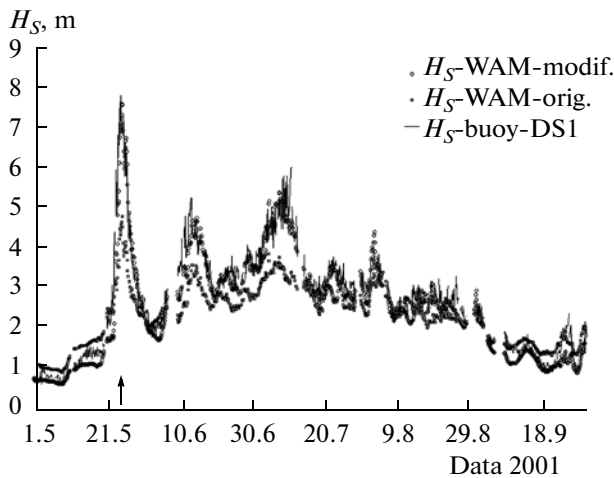


Fig. 6. The time history of significant wave height $H_S(t)$ at buoy DS1 for the period from May to September 2001: the thin solid line is the data of the buoy measurements, squares are the results of calculations with the original WAM model, and circles are the results of calculations with the modified WAM model. The arrow shows the beginning of the summer monsoon over the south of the Indian peninsula.

0.25% per year and the presence of a fairly significant trend for the density of mean-over-ocean wind energy flux: the increase is 1% per year. Note that the first digit of the trend clearly falls into the confidence interval, having an order of 1% (taking into account the variance of the annual wind for 12 years). The statistical trend parameter, which is equal to $R^2 = 0.35$, testifies to the same thing. Meanwhile, the estimate of the trend for FKEW is already in the range of 1% per year and deserves attention ($R^2 = 0.71$).

That is the magnitude of the trend for $E_A(t)$, which is of major interest in the light of the long-term (climate) variability of FKEW in the IO's area. In a view of the smallness of the time period (12 years), these estimates, of course, have a tentative nature (local for these years). However, they are important both for the purposes of their clarification for longer periods and for the purposes of a subsequent comparison of the trends for wind-energy fields, with ones for wave-energy fields representing the main interest of the project.

5.2. Location of Extremes for the Wind Speed

The extreme values of the wind speed W_{\max} and the coordinates of their spatial and temporal distribution are shown in Table 2 of archive [5]. A complete analysis of the table and complete picture of the wind maxima in the form of a "synthetic" map, the points of which are not tied to a single time, are presented there.

5.3. Histograms of the Wind-Speed Distribution (in the Zones and the Whole IO)

The most complete probabilistic information about the wind-speed field is given by its histograms, which have been studied in a lot of papers (see references in [7, 9, 10]). For this reason, the analysis of histograms and their first four statistical moments performed by us is moved out of this text. It is presented in archive [5]. One significant result of this analysis is the strong variability of the statistical moments of the wind-speed statistical distributions both among the zones and depending on the scales of averaging.

6. THE MAIN RESULTS OF THE WIND-FIELD ANALYSIS

The main results concerning the analysis of the wind field in the IO consist of the following.

6.1. The zoning of the IO into 6 zones is established and justified (Section 2, Fig. 1a) and the dynamics of the wind circulation has stable characteristics at all the considered scales of averaging. Using the example of the wind-histograms analysis, it was shown that, due to spatial variability, an estimation of the mean statistical quantities averaged over the whole ocean is not acceptable even for studying the variability of geophysical fields on long-term (climate) scales; i.e., it is necessary to study the statistics in each zone separately.

6.2. A variety of scales of variability both for the "instantaneous" values of the wind at fixed points and for the series obtained at different scales of spatial and temporal averaging are established. The natural enlargement of the main period for wind-field variability from a period of 0.5 year to a period of 1 year while moving through the set of zones to the south is revealed. In the spectra of the "instantaneous" series (with a time-step of 3 h), the following scales of variability (both for the wind speed and FKEW) are fixed: 1 year, 0.5 year, 100 days, 60 days, 40 days, 1 day, 0.5 day, and 0.3 day. Starting from the synoptic scale (10 days or less), the spectra of velocity and energy-flux density for wind power have exponent decay laws with indexes from $-5/3$ to -2.5 (Section 4).

In the spectra for daily mean values of wind speed and energy averaged over the zones and whole area of the ocean, only the scale of 1 and 0.5 year is well marked. In addition, the scales of synoptic variability (5–8 days), which occur against a background of exponential decay of the high-frequency part of the spectrum, are also distinguished. Only these scales are responsible for the visually observed significant synoptic variability of the wind energy (Section 5.1; Figs. 4a–4d).

For the wind-energy flux values averaged over the zones and the whole ocean, the spectrum has the white noise part ("shelf") located between the scales of max-

imal variability (1 year or 0.5 years) and the small scales of a turbulent nature. The shelf part of the spectrum commences on a scale of 100 days and ends on scales of 10–3 days. The presence of the shelf in the spectrum shape indicates the absence of an appreciable dynamic relation between movements in the specified range. At the same time, the dynamics of processes at smaller scales (turbulent transport of energy through a cascade of scales) is similar in all zones, which leads to the conservation of the falling exponent spectra on these scales for all versions of field averaging.

6.3. The estimates of the energy store for the wind field and its variability were found both in the zones and in the whole IO for the first time. For 1998–2009 it was shown that the confident positive trend takes place for the ocean-averaged FKEW, having a value of about 1% per year. Due to the smallness of the analysis period (12 years), these results are preliminary. Nevertheless, they add additional scientific interest to the study of the long-term variability of the atmospheric dynamics.

7. MODIFICATION OF THE WAM MODEL AND OBJECTIVES OF THE WAVE-FIELD STUDY

7.1. Results of the Modified Model WAM Verification

The numerical model WAM (Cycle-4), modified with the new source function proposed in [3], has been used to calculate the wind-wave field in the IO. In this section we briefly review the results of a comparative verification of the modified WAM model performed on the basis of the available data of three buoys located in the area of the IO. Herewith, we will follow the specified technology of data processing that was developed and successfully tested previously [16]. Recall that the numerical model WAM is described by the equation [2]

$$\frac{dS(\sigma, \theta, \mathbf{x}, t)}{dt} = F(S, \mathbf{W}, \mathbf{U}) = In + NI - Dis, \quad (7.1)$$

where the left-hand side is the full derivative in time for the frequency-angular spectrum of wind waves, $S(\sigma, \theta, \mathbf{x}, t)$, and the right-hand side is the so-called source function, F , which depends both on wave spectrum $S(\sigma, \theta, \mathbf{x}, t)$ and the local wind $\mathbf{W}(\mathbf{x}, t)$ and currents $\mathbf{U}(\mathbf{x}, t)$. The left-hand side of (7.1) is the mathematical part of the model. It is achieved in the WAM as a set of programs for calculating the evolution of the wave spectrum in the spherical coordinates with the use of standard initial and boundary conditions. This part of the model remained unchanged in our calculations.

The right-hand side of (7.1) gives a mathematical representation of the source function (SF) summands (terms) defining the physical content of the model. The SF describes the mechanisms of wind-wave evolution: the rate of energy transfer from wind to waves, In ; the rate of nonlinear transfer of wave energy through the spectrum, NI ; and the rate of wave energy dissipation, Dis . Just these terms of the SF of the original model were replaced by the ones proposed in [3].

The details of the modified SF's representation, as well as the technology of comparative verification, have been described in detail previously [16]. Therefore, we present here the final results of the root-mean-square error estimates (r.m.s.), δH_S , for the modeled values of the significant wave height, H_S . This error is obtained by means of comparing the modeled wave heights with those measured on three buoys located in the Arabian Sea (table).

As can be seen from the table, the win of accuracy for the modified model (i.e., the decrease in δH_S) is, on average, about 35% of the errors for the original model. In the terminology of [16], it is an indication of the significant improvement of the model. In our calculations, the average value of δH_S is about 0.35 m for the modified model.

On the example of buoy DS1, the result of comparison of the calculations is visually represented in Fig. 6 (the correlation coefficient of the wave height series on the buoy and obtained by the modified model is 0.95). It is seen that the main win in accuracy is due to the more adequate description of the extreme values of wave height given by the modified model (an explanation of this fact can be found in [4, 16]). This fact allows us to state that the results of calculations of extreme wave height in the IO obtained with the modified model have higher reliability than those obtained with the original WAM model. The same is confirmed by a comparison of histograms of these series (see figures in the annex to archive [17]).

7.2. Setting Tasks for the Wave-Field Analysis

Research objectives for the wind-wave field study in the IO are completely formulated analogously to those for the wind field (see Section 2). The only difference is in the following. In order to obtain the mean wave-height fields $\langle H_S(i, j, T) \rangle$, in formulas (2.1) and (2.3), the wind field $W(i, j, t_n)$ should be replaced by the wave height fields $H_S(i, j, t_n)$ and, in order to obtain the wave-energy fields $\langle E_W(i, j, T) \rangle$ in formulas (2.2) and (2.4) the density of the wind energy flow $\rho_a W^3(i, j, t_n)/2$ must be replaced by the wave energy density $g \rho_w H_S^2(i, j, t_n)/16$ (where g is the acceleration due to gravity and ρ_w is the density of water).

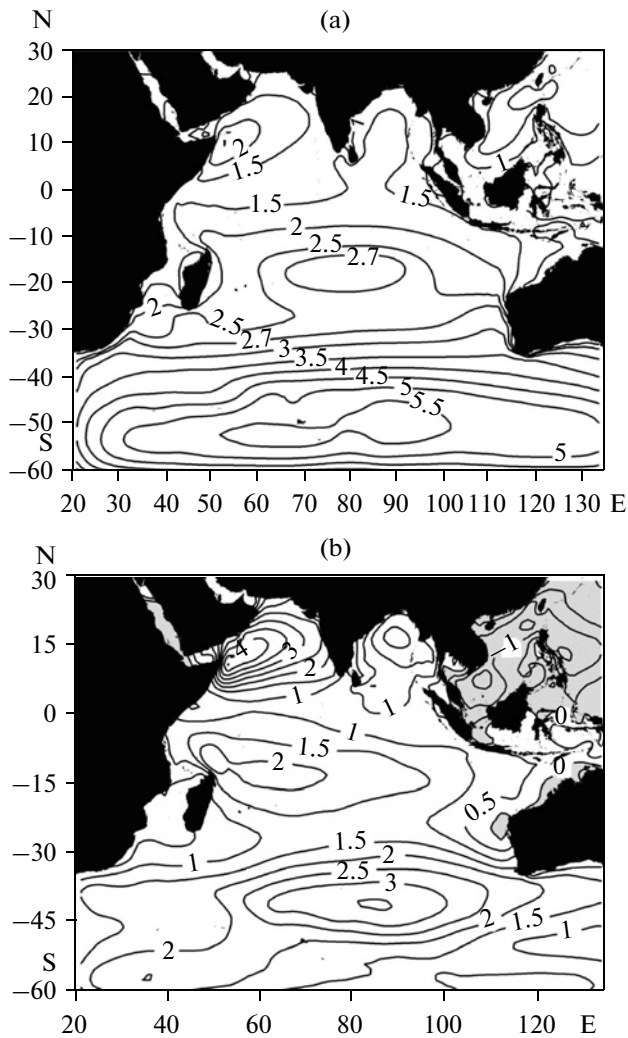


Fig. 7. The charts of calculated fields: (a) the field of wave height H_S averaged for the whole period of 1998–2009; the isolines are numerated in meters. (b) The seasonal difference mean fields (July–January) averaged for the entire period, m. The shaded area corresponds to negative values of the seasonal difference.

Herewith, it is assumed that the field of wave height $H_S(i, j, t_n)$ is calculated with the modified WAM model used for the wind-field grid: $1^\circ \times 1.25^\circ$ in latitude–longitude and 3 h in time. The relation of the significant wave height with the wave spectrum is given by (7.2).

$$H_S(i, j, t_n) = 4 \left(\iint S(\omega, \theta, i, j, t_n) d\omega d\theta \right)^{1/2}. \quad (7.2)$$

In all other respects, all seven objectives formulated in Section 2 are transferred to the formulation of tasks for the wind-wave field analysis in all details. This methodological unity allows us to not dwell on this issue more and to go directly to the analysis.

8. ANALYSIS OF THE CHART FOR WAVES AND THEIR ENERGY

8.1. Charts of the Mean Wave-Height Fields

Out of all the charts for the mean wave-height fields $\langle H_S(i, j, T) \rangle$, the most important two charts are represented for demonstration (Figs. 7a, 7b). More detailed wind-wave fields and the fields of wave energy are represented in archive [17]. A general analysis of the whole variety of charts testifies to the following features of the mean fields H_S .

First, all the charts show a remarkable and sustainable distribution of wave height through the space, shown using the example of the chart averaged for the entire 12-year period (Fig. 7a). Like in the wind field, the same six designated zones characterized by the local extrema of the field $\langle H_S(i, j, T) \rangle$ are seen: the Arabian Sea (Z1), the Bay of Bengal (Z2), the equatorial part of IO (Z3), the southern part of the trade-wind in IO (Z4), the subtropical southern part of IO (Z5), and the southern IO (Z6). The reason for the zoning is provided for the wind dynamics discussed in detail above, which makes it possible not dwell on this issue. Here it is important to note the fact of the sustainable spatial inhomogeneity of all the mean wave-height fields: seasonal, annual, and averaged through the whole period under consideration (see figures in [17]).

Note that, due to the space-time inertia of the wave field, when compared to the variability of the wind one, the zone boundaries for the fields of wave and wind are somewhat shifted and, in the wave field, not all the zones are clearly marked. Nevertheless, in order of succession to the earlier analysis and accounting for insignificant changes in the zones boundaries, further we will use the previously adopted zoning partition of the IO (Fig. 1a and table in [5]).

The second feature deals with the ranging of characteristic values for the wave fields. Note that the 12-year-mean values of H_S range from a minimum value of 1 m in the coastal areas of zones to maximum values on the order of 5.5–6 m in the center of zone Z6 (Fig. 7a). Herewith, the maximum waves are often found in the summer (see [17]). In contrast to the 12-year-mean fields, the seasonal and annual fields, while maintaining the mentioned zoning structure, indicate even a greater range of variability.

Third, it is important to note a very strong seasonal variability of the mean field $\langle H_S(i, j, T) \rangle$, which is shown using an example of the “summer–winter” difference for the 12-year-mean wave fields (Fig. 7b). An increase in the average wave height takes place in summer almost everywhere except for the eastern part of zone Z1. This increase is especially noticeable in the western part of zone Z2 and in the center of the border between zones Z5 and Z6. That differs from positions of maxima for the seasonal variability of the wind

(Fig. 2b). The summer-increase for the wave height can reach 3–4 m, i.e. about 100% of the average winter values. Herewith, the negative seasonal changes in the wave height in the IO during the summer period are almost not observed except for a narrow region near the northwestern coast of Australia. Thus, the monsoon variability of wind, which is the source of seasonal variations in the wave field, is most pronounced only in the northwestern part of the IO.

Finally, a few words about the average wave-height trend for the entire period (Fig. 2c in [17]). The regularity of the average height distribution through the zones is practically repeated in the field of its time trend, which was obtained by the method of least squares for each point of the wave fields taken with time increments of 3 h (“instantaneous” fields). Compared with the same trend of the wind field (Fig. 2c in [5]), the wave trend field, which was found even for the “instant” wave height, is characterized by a greater smoothness. That fact is determined by the inertia of a wave field.

For the whole 12-year period, the average increase in wave height with a rate of about 1% per year (which exceeds the limits of the confidence interval of variability, having a value of about 0.3–0.5%) is seen. The trend is most pronounced in areas of high winds (zones Z2, Z4, and Z6). It is important that the magnitude of the mean trend of “instantaneous” wave fields of 1% corresponds to the trend for the annual values of H_5 averaged across the ocean (see Section 10).

Regarding the negative trends of wave height, a more reliable determination (and explanation) of them demands a longer period of simulations and a separate discussion.

8.2. Charts of the Wave Energy

Charts of the wave energy $\langle E_w(i, j, T) \rangle$ are defined by the wave-height fields. This means that the mean wave-energy fields $\langle E_w(i, j, T) \rangle$ are rather similar to the mean-height fields, $\langle H_5(i, j, T) \rangle$, emphasizing essentially the areas of extreme waves. Nevertheless, a separate calculation and analysis of variability for the wave-energy fields has its own justification. As was noted in Section 3, the importance of wave-energy fields $\langle E_w(i, j, T) \rangle$, as well as the fields of the flow of kinetic energy of wind, $\langle E_A(i, j, T) \rangle$, are determined by their importance in describing the atmosphere–ocean interaction. For this reason, we put the study of the wave-energy and wind-energy fields and their variability as the basis of our research, taking into account that these fields determine the intensity of the mechanical energy transfer from wind to waves, the analysis which we plan to perform in subsequent papers. To our

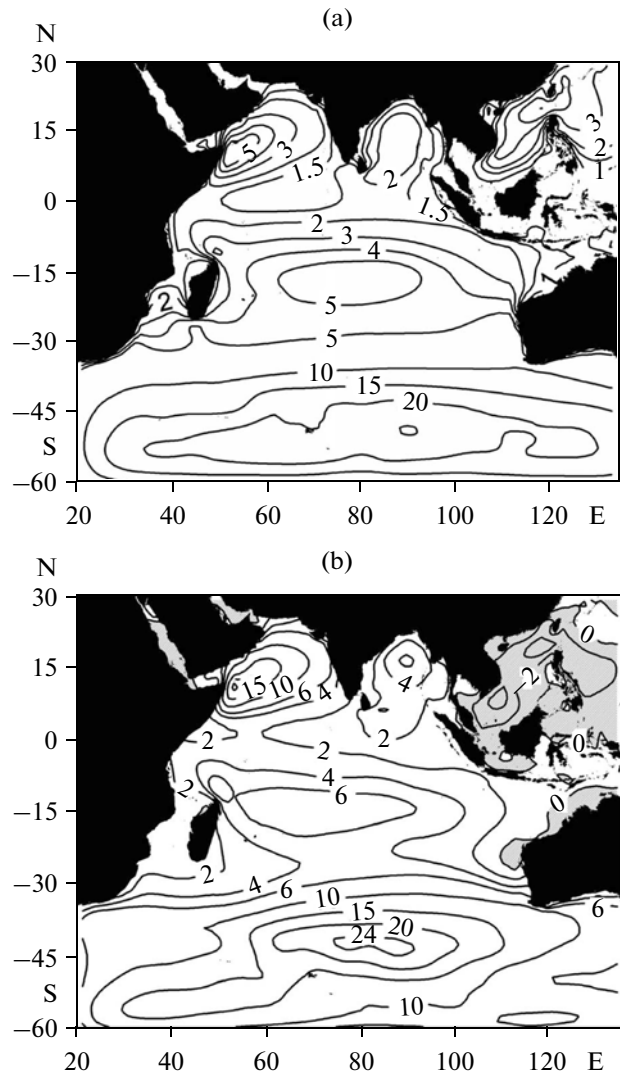


Fig. 8. The same as in Fig. 7 but for the mean wave energy; the plots are given in units of kJ/m^2 .

knowledge, there are no analogues of such calculations or their analysis in the literature.

The most important results of calculations of the wave-energy fields are shown in Figs. 8a and 8b (and in more detail in [17]). In comparison with the fields of wind energy, these results indicate the following features of fields $\langle E_w(i, j, T) \rangle$.

First and foremost, note that the zone-structure of the fields $\langle E_w(i, j, T) \rangle$ is retained at any time-scales of averaging (seasons, years, the entire period), and the peculiarities of their spatial distribution becomes more exaggerated. Thus, for field $\langle E_w(i, j, T) \rangle$, averaged for the whole 12-year period, the range of variability reaches 20 units, i.e., 4–5 times greater than one for field (compare Figs. 7a and 8a). At most, the characteristic value of the 12-year-mean wave energy reaches by 20 kJ/m^2 , whilst the minimum values are on the

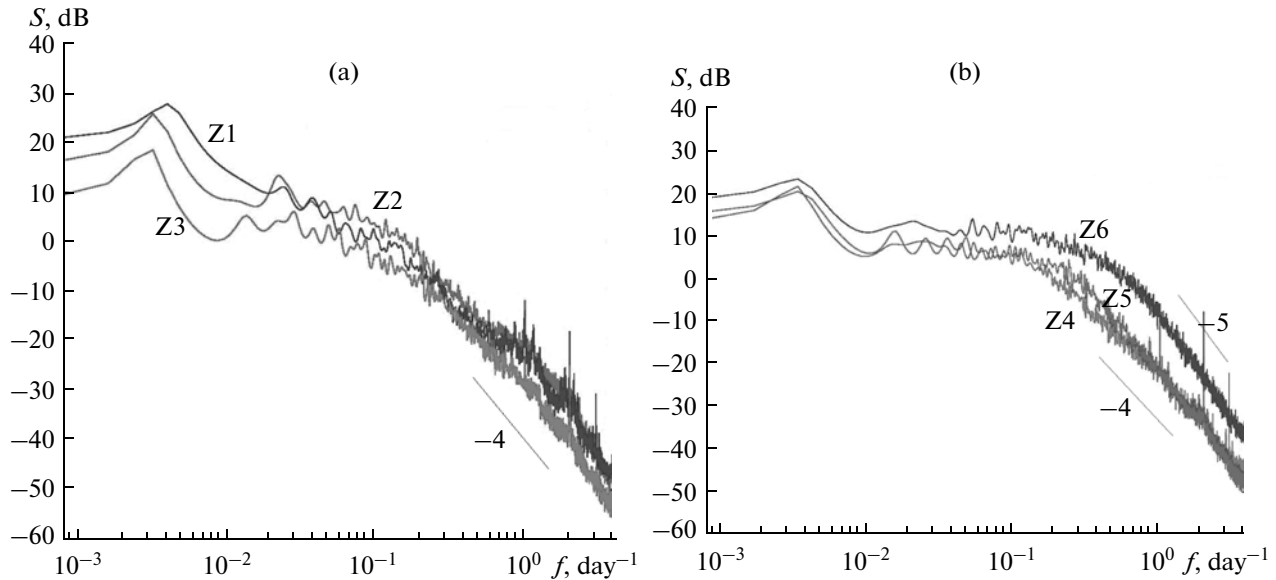


Fig. 9. The spectra of 3-h series for wave height at the central points of the IO zones (see table): (a) zones Z1–Z3; (b) zones Z4–Z6.

order of several units of kJ/m^2 (in the coastal areas and throughout zone Z3).

The consistency of geometry for fields $\langle H_S(i, j, T) \rangle$ and $\langle E_w(i, j, T) \rangle$ is seen for all scales of time averaging. Therefore, in view of a detailed description of the wave-height fields given above, a further description of details for the wave-energy fields $\langle E_w(i, j, T) \rangle$ will only require some specification. In particular, to describe the temporal variability of the wave-energy field, it is sufficient to give quantitative estimates of trends for its seasonal and long-term variability.

Thus, the range of seasonal “summer–winter” variability (Fig. 8b) is from 25 kJ/m^2 (at the maximum, corresponding to the center of zone Z6) to 2 kJ/m^2 (at a minimum, covering the whole equatorial zone Z3). These values indicate a double increase in wave energy in the summer period, which takes place almost throughout the whole IO.

The interannual 12-year trend of “instantaneous” wave-energy fields has a range of variability from zero (at the border of zones Z1–Z2–Z3 and in the south of the Indian peninsula) to values of 500 J/m^2 in the center of zone Z6 (Fig. 2c in [17]). Thus, for the specified long-term period, the trend is about 2% per year (the average value for the entire period). Herewith, the main increase in energy takes place in the western and eastern parts of zone Z6. The zero trend in the area to the south of the Indian peninsula is an unexpected feature of the field $\langle E_w(i, j, T) \rangle$, a justification for which should be sought in the overall dynamics of atmospheric circulation.

Comparing the average values of the wind kinetic-energy fluxes (on an order of 1000 W/m^2) with the average values of wave energy (on the order of 10^4 J/m^2) and taking into account the estimate of the energy-transfer rate from wind to waves obtained in [12] and having the order $C_d^{3/2} \sim 10^{-4}$, one can find that the “full pumping” of ocean waves by wind (in the stationary case) could be achieved during a time on the order of 10^5 s , i.e., on the order of a day. This result suggests the possibility of a sufficiently rapid dynamics of the wind-wave energy transfer (taking into account the scale of the ocean). It will be shown (Section 9) that such a dynamics is actually achieved, but the scales of its variability have somewhat larger values (7–10 days). The obvious reason for this increase in the pumping scale of the ocean waves by the wind is the heterogeneity and nonstationarity of the latter.

In summary, note that the above estimates are new results in studies of the variability of wave fields in the IO. It is natural to expect that such work in this direction needs to be continued, which may result in some refinement of these estimates.

9. ANALYSIS OF THE TIME-HISTORY OF WAVES AND THEIR ENERGY: THE SCALES OF THEIR VARIABILITY

9.1. The Time History of Wave Height at the Fixed Points of the Zones

Let us first consider the time-history of the “instantaneous” wave height at the “central” points of the IO zones, the location of which is shown in Fig. 1a (for the exact coordinates, see the table of archive

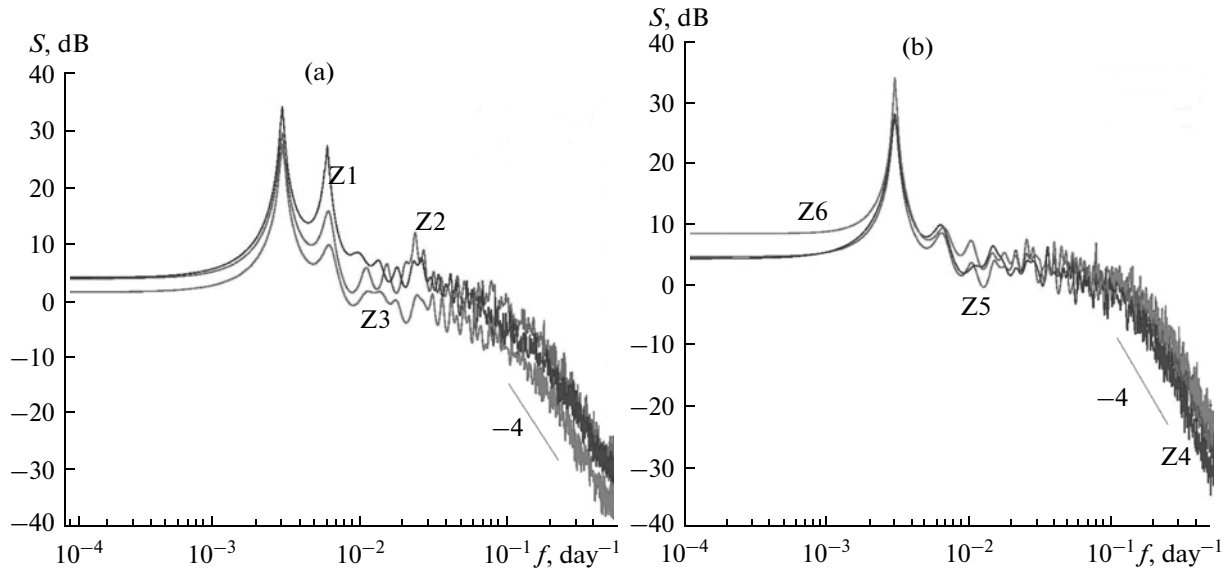


Fig. 10. The spectra of the daily series of wave height averaged over the zones of the IO (see table): (a) zones Z1–Z3; (b) zones Z4–Z6.

[17]). Such an approach is important to determine the full range of temporal variability scales of the wave field and its variations while moving from north to the south. Only the main results are represented here (for details, see [17]).

A visual analysis of the 3-h series (Fig. 3 in the annexation to [17]) shows a series of differences between the wave and wind fields. The most important of them is that the annual harmonic is the most pronounced in all the zones (whilst in the time series of the wind field, the semiannual harmonic is the most visible; see [5]). At the same time, in the northern zones of the wave field (as in the wind fields), the variability on the scales of several tens of days is clearly visible, which is changed by the variability on smaller scales while moving to the south. These observations are fully confirmed by the results of spectral processing series $H_S(Z_I, t)$, which was performed on the basis of the autoregressive Yule–Walker analysis [14]. The latter has confidence intervals on the order of $\pm(10–20)\%$ in the logarithmic scale.

From an analysis of the frequency spectra shown in Figs. 9a and 9b, one can draw the following conclusions. For zones Z1–Z3, which have a similar dynamics (Fig. 9a), the largest variability takes place in the period of one year, which, with an increase in the frequency, is followed by a cascade of weakly expressed scales from 30 to 10 days slowly decreasing in intensity. Starting with a period of 10 days, the wave-height spectra take on a fast-falling feature similar to form $S(f) \propto f^{-n}$ with the exponent $n \cong 3.5–4$. Such high degrees of spectrum decay (compared with the values of $n \cong 1.5–2$ for the wind spectrum; see Section 4) are

evidently given by the nonlinear dependence of wave height on the wind speed (see [16]). In addition, it is important to note the pronounced maxima of the spectrum for wave height on scales of 1, 0.5, and 0.3 days, repeating the same extremes in the spectrum of the wind (Section 4). For the southern zones Z4–Z6, the spectra of waves (Fig. 9b) are qualitatively similar to the spectra for the northern zones. However, the cascade of falling intensities is transformed to the shelf of the white noise spectrum, which occupies the scale from 100 to 10 days and completely repeats the shape for the proper wind spectrum (Section 4). As was suggested earlier, such a shelf is a consequence of a lack of correlation for wind variability on these time scales, which naturally affects the variability of the wave height.

9.2. The Time History of Wave Energy at the Fixed Points of Zones and Its Spectrum

It is interesting to compare the above results with their counterparts for wave-energy series $E_W(Z_I, t)$. In this case, as far as the time history $E_W(Z_I, t)$ repeats the time history of wave height $H_S(Z_I, t)$ which increased in amplitude exaggeration, of main interest is not the series but their spectra.

The calculations performed have shown that the energy spectra are similar to those of the spectra of height, differing mainly by the magnitude of their intensity (not shown). In this respect, the wave-energy spectra are less interesting than the wind-energy spectra, which indicated a larger set of variability scales (see Section 4 and [5]). Apparently, this “poorness” of scales in the wave-energy spectra is due to the higher

inertia of the wave field smoothing small scales of variability of the time history for wind energy.

Another difference between the wave-energy spectra and ones for the wave height, in addition to their intensity, is the increase in degree of the spectral decay on 15–20% for the range of periods from 10 days and down. In this range, the decay exponents of the energy spectra $S(f)$ have values $n \cong 4.5-5$. The above gives a complete description of both the series and the wave-energy spectra, which allows us to not dwell on it here in detail.

9.3. Spectra of the Wave Height Averaged for One Day and over the Zones

An analysis of data of this kind reveals a significant difference between the spectra for the averaged wave height from the spectra for “instant” height (Fig. 9), which consists of the following (Fig. 10). As was seen from Fig. 10a, for the specified series, in the northern zones Z1–Z3, in addition to the prevailing scale of variability of 1 year, the marked semi-annual variability takes place similar to that for the wind fields (Section 4). As one moves south, this variability gradually wanes, almost disappearing in zones Z4–Z6 (Fig. 10b).

The reason for the semiannual variability disappearance in the wind fields (and hence in the wave ones) is the same: the northern zones of the IO fall in the tropics. There, the sun crosses the zenith twice a year. As one moves to the south (into the middle latitudes), the effect of the “double zenith” disappears and the reason for semiannual harmonics vanishes.

This behavior of the variability indicates a synchronism of the semiannual variations for wave height in the zones as a whole, which manifests itself in the spectra of the averaged series. At the same time, at the central points of the zones, as we have seen, this scale of variability does not occur (within the confidence intervals).

For the northern zones, credible peaks of intensity on a 30-day scale are clearly visible. In the southern zones, similar peaks occupy a larger range of scales, appearing on the background of a long shelf extending on the scales from 100 to 10 days. These scales of variability are not very pronounced; however, they deserve to be mentioned. It is not excluded that this is a display of the multiple harmonic of the annual fluctuations offered by the nonlinear nature of wind waves. However, in general, the transfer of energy through the scales ranging from 100 to 10 days does not take place, which is characterized by the presence of a shelf in the intensity of the spectrum in this frequency range. Further studies are evidently needed to clarify the nature of these features for the spectrum of averaged wave-height series.

Regarding the slopes of the spectra in the high-frequency region (for periods of less than 10 days), these slopes do not differ from those for the “instantaneous” wave height ($n \cong 4.5-5$). This behavior of the spectra for averaged series shows a similarity of wave and wind dynamics on these scales (Section 4).

In concluding this sub-section, note that the spectra for the series of wave energy, averaged for one day and over the zones, are in practice slightly different from those for the series of an average height. Therefore, they are not discussed here.

9.4. The Time History of Wave Height and Their Energy Averaged for One Day and over the Whole IO

Let us consider now the peculiarities of the time history and the spectra of the daily mean values $H_S(R, T, t)$ and $E_W(R, T, t)$ averaged over the whole IO (Fig. 11).

First, with respect to the series themselves, it is essential to point out that, despite the large scale of spatial averaging, the time-history of averaged magnitudes $H_S(R, T, t)$ and $E_W(R, T, t)$ shows very strong variability. Therefore, on a scale of several days (5–10 days), the average-over-the-ocean wave height $H_S(R, T, t)$ can vary up to a factor of 1.5–2, and the average wave energy does this 3–4 times (Fig. 11a). Such a strong variability of wave energy for the whole ocean seems to be a much unexpected result, since it shows an intense wave dynamics. Moreover, this variability is typical for the entire period of 12 years under consideration (Fig. 11b). Herewith, the tendency of growth for the wave energy averaged for a year can even be seen visually (Fig. 11b). The estimates explaining the possibility of the “complete” pumping of the wind waves on a scale of 1–2 days have been given earlier in Subsection 8.2. Here, this effect is confirmed visually for the mean-of-ocean values of $H_S(R, T, t)$ and $E_W(R, T, t)$. However, the modeled data offer a 3–4 times greater duration of the ocean “pumping,” which is a significant refinement of the purely theoretical estimates of Subsection 8.2. It is clear that the time-scale increase of the pumping waves by wind is due to the strong inhomogeneity and nonstationarity of the wind field. The importance of the above series is that they give a more realistic assessment of this scale. Second, the spectrum of the wave-height series averaged over the whole IO (Fig. 11c) has a single well-defined period of 1 year against the background of which the semiannual harmonic is almost negligible, although its intensity exceeds the confidence intervals. In this respect, the spectra of height differ from the spectra of wind, in which the semi-annual harmonic was significant even for the whole IO (Figs. 4c, 4d). As the frequency increases, there is already a known lengthy shelf of the spectrum intensity from periods of

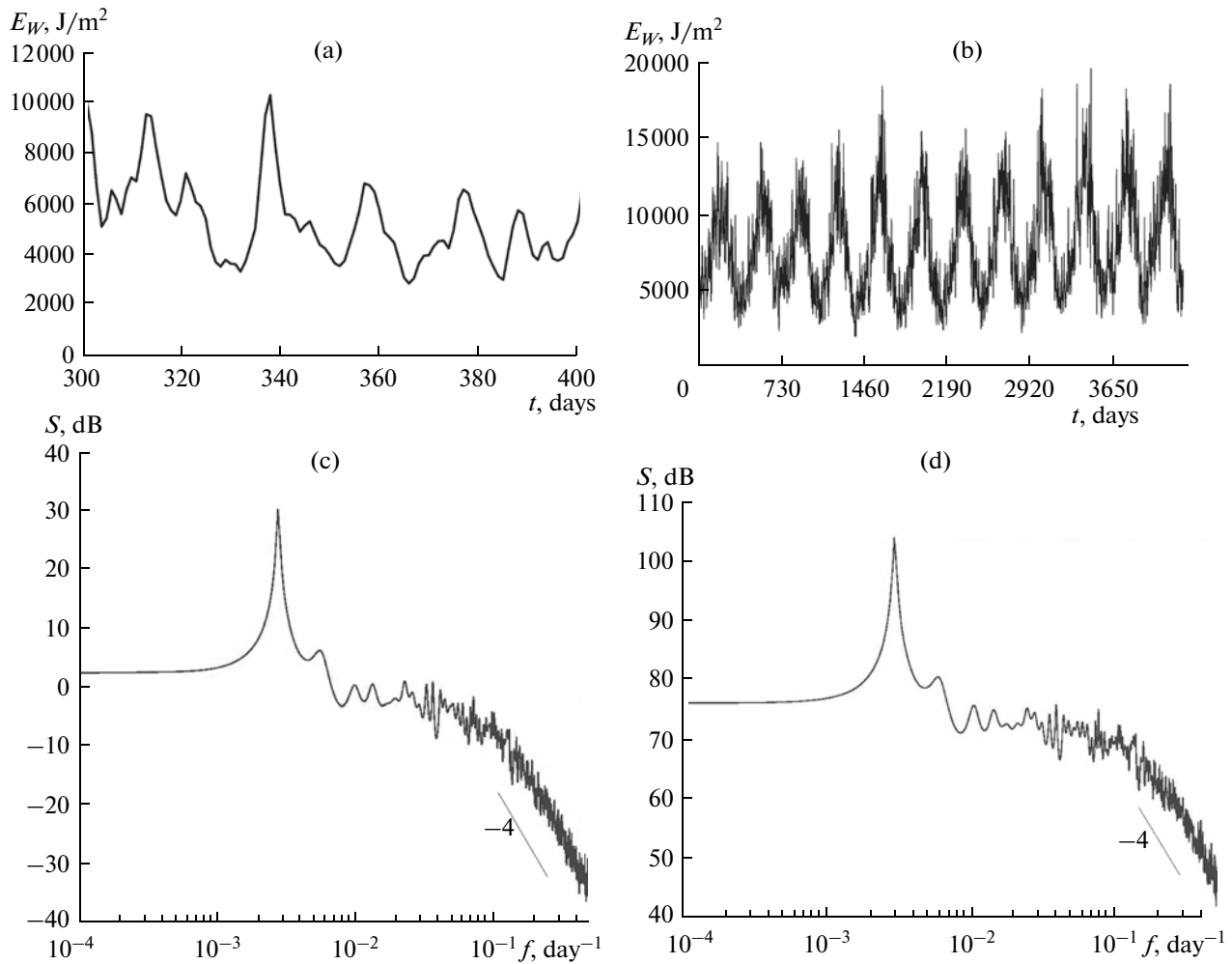


Fig. 11. The series of wave energy averaged for a day and over the whole IO: (a) detailed view of the series; (b) general form of the series. The spectra of daily series of (c) wave height and (d) energy averaged over the whole IO.

100 days to 10 days, on the background of which there are reliable peaks of the spectrum corresponding to scales of 20, 15 and 10 days (these scales are visible in Fig. 11c). Starting from the period to 10 days, the slowly decaying spectrum is replaced by a rather sharp power-law-decay one with an exponent $n = 4$. Here-with, on the tail of the spectrum, selected scales of 7–8 days and 3–5 days, which are well manifested in the spectrum of the wind (see Section 5), are only weakly visible. Third, the spectrum of the wave-energy series averaged for one day and over the whole ocean (Fig. 11d) is similar in all details to the mean wave-height spectrum shown in Fig. 11c. Here they are given only to show their difference from the analogue spectra of the wind energy, which have a larger set of variability scales (see archive [5]).

10. ANALYSIS OF THE INTEGRAL AND LOCAL CHARACTERISTICS OF THE WAVE FIELD

10.1. The Time History of the Annual Values for Wave Height and Their Energy

The two panels of Fig. 12 show the time history for the annual values (averaged over all zones and the IO) for the wave height (Fig. 12a) and their energy (Fig. 12b). The expected distribution of the mean values among the zones is seen. It is interesting to note that estimates of the annual values of energy among the zones (with an error of about 10%) correspond to the relation of the form $E_w(R, T) \cong 1000 H_S^2(R, T)$. This empirical fact can be used to obtain fast “expert” estimates of the mean energy of waves without involving cumbersome calculations.

Limited by the analysis of integral values for the whole IO, the presence of a well discernible trend for

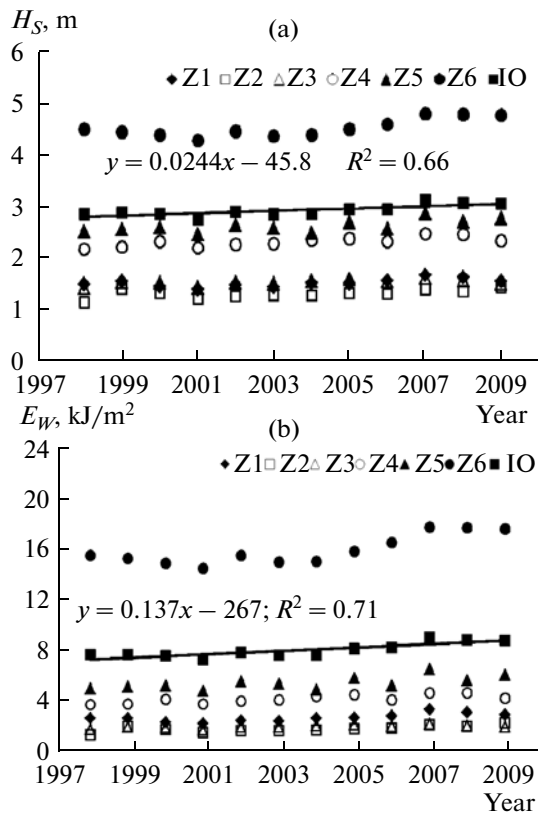


Fig. 12. The time history of the annual (a) wave heights and (b) energy averaged across the zones and the whole IO. The r.m.s trend lines for the entire IO and their formulas are shown.

the mean wave height should be noted in Fig. 12: growth on the order of 1% per year, which corresponds to the limits of the confidence intervals for the variability of the series ($R^2 = 0.66$). This trend is accompanied by an even more pronounced trend of the ocean-mean energy of waves: growth on the order of 2% per year, which already exceeds the confidence intervals ($R^2 = 0.72$) and can be regarded as a reliable result. Just these values of trends are of major interest in view of establishing the long-term variability of wave energy in the IO area. Naturally, due to the small time period (12 years), the estimates obtained here have a local (i.e., nonclimate) feature. Nevertheless, they are important both for the purposes of clarification for longer periods of analysis and for comparison with the similar trends of wind energy.

Thus, there is a rather good agreement between all the trends: the trend for the density of the wind-energy flux obtained previously was about 1% per year (Section 5), which correlates rather well with the growth of the wave height of 1% per year and one for the wave energy of 2% per year.

It should be especially emphasized that this kind of detailed numerical estimates for the energy of the wave

field in the IO have no analogues. Therefore, we believe that the estimates are of significant interest both for scientific and practical aims. This issue is discussed in more detail in the concluding Section 11.

10.2. The Location of the Wave–Height Extrema

The extreme values of wave height H_{\max} and the coordinates of their spatial and temporal distribution (i_m, j_m, t_m) are shown in Table 3 of archive [17]. As was mentioned above, these space-time coordinates are of interest for comparison with the similar coordinates of the wind-speed maxima. A joint analysis of the tables for the wind and wave maxima is given in [17].

10.3. Histograms of the Wave–Height Distribution in the Zones and the Entire IO

The most complete probabilistic information about the field of wave height is given by histograms, the study of which is considered in a lot of papers (see references in [7, 18]). Histograms are the numerical representation of the probability density function (PDF), and, for a variety of geophysical fields, they are usually parameterized by one or another kind of Weibull's distribution [7, 10]. In terms of the stationary and unmixed wave state, the instant wave heights are well described by the Rayleigh distribution [18], which is a special case of the Weibull's distribution. However, it is important to note here that we are dealing with the PDF applied not for a series of random wave heights, but namely with the PDF for certain statistical characteristics of the field: the significant wave height defined via the wave spectrum by Eq. (7.2). Therefore, we cannot expect a distribution close to Rayleigh's PDF. These differences make up the main interest of our estimations.

It is known, however, that the PDF parameters for the waves do strongly depend on the conditions of wave formation [7, 18]. Therefore, one should expect that, on the scales of the IO, these parameters will vary considerably both in space and time and depend also on the scales of the space-time averaging of the wave field. This variability in the probabilistic structure of the wave-height field leads to the necessity for separate direct calculating parameters of Weibull's distribution for each of the selected areas and time periods. The full discussion of this problem requires a separate presentation. In our task it is presented in Section 5 of archive [17].

11. THE MAIN RESULTS OF ANALYSIS FOR THE WAVE FIELD

The most important results of an analysis of variability for the wind-wave field in the IO are the following.

11.1. Despite the nonlocal dependence of the wave field on the wind field, it is shown that the zoning of

the wave field in the IO area can be, in general, linked to the previously adopted zoning for the wind field (Sections 2 and 8). On this basis, the analysis of the variability scales for the wave field is performed separately for each zone (Sections 8–9), whilst the annual ocean-mean values are analyzed only in order to determine the 12-year variability of the wave field (long-term trends of wave height and their energy averaged over the whole IO, Section 10.1). The probability statistics are the most reliable when they are constructed for each zone separately (section 10.3).

11.2. A spectral analysis of the wave series obtained for different scales of averaging (Section 9) shows that the main scale of variability is one year. Against this background there is variability with a period of 0.5 year and a number of scales in the range of 40–10 days. Herewith, the period of 0.5 year is typical only for the northern zones Z1–Z3.

For the southern zones Z4–Z6, there is a weak variation in the spectra intensity in the range of periods from 100 to 10 days. This peculiarity of the spectra shape for the wave height resembles the same feature of the wind speed spectra (Section 4). That allows us (by analogy) to treat it as a manifestation of the lack of correlation for the wave-field variability in this range of scales.

In the range of 10 days and less, for all scales of averaging of the wave field, there is a power-law decay for the spectrum of wave height series with decay parameters $n = -(3-4)$ and for the wave-energy spectra with $n = -(4-5)$. More detailed conclusions about the variability scales and an interpretation of the spectra shapes are given in Section 4.5 of archive [17].

11.3. The estimates of seasonal, interannual, and 12-year variability were obtained for the wave height and wave energy fields. For the first time it was found that, for 1998–2009, there is a positive trend of the ocean-mean wave height of about 1% per year, as well as for the wave energy on the order of 2% per year. This result correlates well with the previously established value of the trend for FKEW of 1% per year (Section 6).

12. CONCLUSIONS

In conclusion, we should refer to the freshest data obtained in this direction and presented in recent paper [19]. These results indicate that estimates of the average trends for the World Ocean mean wind speed and wave height made on the basis of a long-term analysis of satellite data are 2–3 times lower than those obtained by us. This difference gives rise to a number of tasks. One of them is associated with the specification of the range of reliable values of remote sensing data, and the second is associated with the specification of reliability for the numerical modeling results. Leaving the discussion and solution of these princi-

pally important issues for future, note that it is this difference that increases the significance of the estimates obtained in this paper, the clarification of which becomes a necessary and urgent continuation of the work in this direction.

ACKNOWLEDGMENTS

We are grateful to the head of the Division of Atmospheric Dynamics, Institute of Atmospheric Physics, Russian Academy of Sciences (RAS), G.S. Golitsyn for our many discussions of the results and the appendix that he provided. We also thank project manager A.S. Ginzburg for extensive support of the work and for resolving the issues that arose during the project. We are grateful to I. Mokhov for having permanent interest in this work. This work was supported by the Russian Foundation for Basic Research, grant no. 10-05-92662-IND_a.

APPENDIX “(by G.S. Golitsyn)”

Emphasis is placed on the power-law parts in the spectra for wind speed (Figs. 3a, 3b, 4c) and the third statistical moment of it: the density of flux for the kinetic energy (Fig. 4d) (presented in [5] in more detail). They take decades for frequencies with periods from about 10 days to a day. Herewith, the slopes of the spectra for the individual zones are slightly different, and the FKEW spectra are steeper than the spectra of wind velocity. Their slopes are “–2” and “–2.5,” respectively. These slopes are valid for the spectra of currents in the Lagrangian description of turbulence [15]. It is interesting to get such parameters theoretically. Indeed, the temporal structure functions for the second-order velocity have the form [15]

$$D_2(\tau) = \langle [u(t+\tau) - u(t)]^2 \rangle = \varepsilon\tau, \quad (\text{A1})$$

which follows from the dimensional considerations. Here ε is the energy flux through the spectrum of scales. For the same reason, following kind of structural function of the third order is obvious:

$$D_3(\tau) = \langle [u(t+\tau) - u(t)]^3 \rangle = (\varepsilon\tau)^{3/2}. \quad (\text{A2})$$

The spectra are found from the relation [15]

$$D_n(\tau) = \int S_n(f)(1 - \cos(f\tau))df. \quad (\text{A3})$$

They also have a power-law shape; herewith their negative exponents are more than unity with respect to ones for the structure functions. Thus, the spectrum of the second order will be $S_2(f) \sim f^{-2}$ and the spectrum of the third order is $S_3(f) \sim f^{-2.5}$.

The proposed consideration is in no way proof, since the data of the wind reanalysis (or buoy measurements) give the value of the field at a point, i.e., they

are neither Eulerian nor Lagrangian velocity. The wind is heterogeneous not only in magnitude but also in direction throughout the 10 days mentioned in which there are the parts of power spectra; i.e., there is no statistical homogeneity there. Nevertheless, the existence of the power-law parts in the time spectra of the wind-speed statistical moment is interesting in itself, because it gives a basis for analyzing the reason that it can occur. The above estimations indicate such a possibility.

REFERENCES

1. <ftp://polar.ncep.noaa.gov/pub/history/waves/>
2. The WAMDI Group, "The WAM—A Third Generation Ocean Wave Prediction Model," *J. Phys. Oceanogr.* **18** (12), 1775–1810 (1988).
3. V. G. Polnikov, "Wind-Wave Model with an Optimized Source Function," *Izv., Atmos. Ocean. Phys.* **41** (5), 594–610 (2005).
4. V. G. Polnikov, V. Innocentini, "Comparative Study Performance of Wind Wave Model: WAVEWATCH—Modified by the New Source Function," *Eng. Appl. Comput. Fluid Mech.* **2** (4), 466–481 (2008).
5. V. G. Polnikov, F. A. Pogarskii, and S. A. Sannasiraj, "Statistical Features of the Wind over the Indian Ocean for the Period 1998–2008" (2011). <http://arxiv.org/pdf/1109.5073>
6. S. K. Gulev, V. Grigorieva, "Last Century Changes in Ocean Wind Waves Height from Global Visual Wave Data," *Geophys. Res. Lett.* **31**, L24302 (2004). doi 10.1029/2004GL21040
7. *Handbook of the Register for Wind and Wave in the Bering and White Seas*, Ed. by A. V. Lopatukhin, A. V. Bukhanovskii, and E. S. Chernyshova (The Russian Shipping Sea Register, St. Petersburg, 2010 [In Russian]).
8. S. Caires and A. Sterl, "100-Year Return Value Estimates for Ocean Wind Speed and Significant Wave Height from the ERA-40 Data," *J. Climate* **18** (4), 1032–1048 (2005).
9. E. Bauer, "Characteristic Frequency Distribution of Remotely Sensed *in situ* and Modeled Wind Speed," *Int. J. Climatol.* **16**, 1087–1102 (1996).
10. A. H. Monahan, "The Probability Distribution of Sea Surface Wind Speeds. Part I: Theory and Sea Winds Observations," *J. Climate* **19** (2), 497–520 (2006).
11. V. G. Polnikov, "The Role of Wind Waves in Dynamics of the Air–Sea Interface," *Izv., Atmos. Ocean. Phys.* **45** (3), 346–356 (2009).
12. G. S. Golitsyn, "The Energy Cycle for Wind Waves on the Ocean Surface," *Izv., Atmos. Ocean. Phys.* **46** (1), 6–13 (2010).
13. P. Källberg, P. Berrisford, B. J. Hoskins, et al., ECMWF ERA-40 Atlas. ERA-40 Project Report Series, No. 19 (2005). http://www.ecmwf.int/publications/library/ecpublications/_pdf/era/era40/ERA40_PRS19_rev.pdf
14. S. M. Key and S. L. Marple, "Spectrum Analysis—A Modern Perspective," *Proc. IEEE* **69** (11), 1380–1419 (1981).
15. A. S. Monin and A. M. Yaglom, *Statistical Hydromechanics*, Vol. 2 (Nauka, Moscow, 1967) [In Russian].
16. V. G. Polnikov, "An Extended Verification Technique for Solving Problems of Numerical Modeling of Wind Waves," *Izv., Atmos. Ocean. Phys.* **46** (4), 511–523 (2010).
17. V. G. Polnikov, F. A. Pogarskii, and S. A. Sannasiraj, "Modeling and Analysis of the Wind-Waves Field Variability in the Indian Ocean during 1998–2009 Years" (2011). <http://arxiv.org/pdf/1109.6542>
18. I. N. Davidan, L. I. Lopatukhin, and V. A. Rozhkov, *Wind Waves as the Probabilistic Hydrodynamic Process* (Leningrad, Gidrometeoizdat, 1978) [In Russian].
19. I. R. Young, S. Zieger, and A. V. Babanin, "Global Trends in Wind Speed and Wave Height," *Science* **332**, 451–455 (2011).